EFDA–JET–PR(10)71

N. Hayashi, V. Parail, F. Koechl, N. Aiba, T. Takizuka, S. Wiesen,
P.T. Lang, N. Oyama, T. Ozeki and JET EFDA contributors

Integrated Simulation of ELM Triggered by Pellet through Energy Absorption and Transport Enhancement

Integrated Simulation of ELM Triggered by Pellet through Energy Absorption and Transport Enhancement

N. Hayashi[1], V. Parail[2], F. Koechl[3], N. Aiba[1], T. Takizuka[1], S. Wiesen[4], P.T. Lang[5], N. Oyama[1], T. Ozeki[1] and JET EFDA contributors*

JET-EFDA, Culham Science Centre, OX14 3DB, Abingdon, UK

[1]Japan Atomic Energy Agency, Naka, Ibaraki-ken 311-0193, Japan
[2]EURATOM-CCFE Fusion Association, Culham Science Centre, OX14 3DB, Abingdon, OXON, UK
[3]Association EURATOM-ÖAW/ATI, Atominstitut, TU Wien, 1020 Vienna Austria
[4]Institute of Energy and Climate Research – Plasma Physics, Forschungszentrum Jülich GmbH, Association EURATOM-FZJ, 52425 Jülich, Germany
[5]Max-Planck-Institut fur PlasmaPhysik, EURATOM Association, Boltzmannstrasse 2, 85748 Garching, Germany
** See annex of F. Romanelli et al, "Overview of JET Results", (23rd IAEA Fusion Energy Conference, Daejon, Republic of Korea (2010)).*

Preprint of Paper to be submitted for publication in
Nuclear Fusion

ABSTRACT.
Two integrated core / scrape-off-layer / divertor transport codes TOPICS-IB and JINTRAC with links to MHD stability codes have been coupled with models of pellet injection to clarify effects of pellet on the behavior of Edge Localized Modes (ELMs). Both codes predicted the following two triggering mechanisms. The energy absorption by the pellet and its further displacement due to the E×B drift, as well as transport enhancement by the pellet, were found to be able to trigger the ELM. The ablated cloud of pellet absorbs the background plasma energy and causes a radial redistribution of pressure due to the subsequent ExB drift. Further, the sharp increase in local density and temperature gradients in the vicinity of ablated cloud could cause the transient enhancement of heat and particle transport. Both mechanisms produce a region of increased pressure gradient in the background plasma profile within the pedestal, which triggers the ELM. The mechanisms have the potential to explain a wide range of experimental observations.

1. INTRODUCTION

The energy loss caused by Edge Localized Modes (ELMs) is crucial for the erosion of divertor plates, plasma confinement and control for a steady state in tokamaks. Pellet injection is considered as one possible method to increase the ELM frequency and to reduce energy loss during the ELM. A few ideas have been already explored in attempts to explain ELM triggering by pellet [1,2]. The triggering mechanisms, however, are not fully understood yet.

Multi-machine experiments showed a wide range of phenomena, which follow pellet ablation [1,3-7]. This includes very prompt ELM onset at the time when the pellet passes the pedestal region [5], ability to trigger the ELM with the high repetition rate by the pellet injected from any location [1], a slight decrease (~10%) in the electron temperature along the pellet penetration path before the density increase [6], and a magnetic perturbation induced by the pellet observed even in non-ELMing H-mode and L-mode plasmas [3,7]. The last two phenomena are proposed as candidates of ELM triggering mechanism, which triggers fast global perturbation spreading over the whole flux surface with the electron thermal or Alfven speed [7]. Experimental observations indicate that pellet ablation clouds may absorb the energy of background plasma and transport it to the outward direction of major radius R by the E×B drift, which results from a vertical curvature and ∇B drift current induced inside the clouds by the 1/R toroidal field variation [8]. Further, the sharp increase in local density and temperature gradients close to an ablated cloud generate a wide spectrum of MHD perturbations, which could temporarily increase local heat and particle transports in the background plasma. Turbulence simulations with linear GS2 and nonlinear CUTIE codes for measured profiles just after the pellet deposition in MAST showed that the pellet modified profiles could increase the level of micro-turbulence [9]. The aim of this paper is to model predictively these mechanisms and find out if they can reproduce the main experimental observations.

The integrated simulation code is one of the most effective methods to study the ELM mechanism [2,10,11]. For example, an integrated code COCONUT, which couples a 1.5 dimensional (1.5D)

core transport code JETTO with a 2D Scrape Off Layer (SOL) / divertor code EDGE2D and is now included into larger suite of transport and MHD codes JINTRAC (JET INtegrated suite of TRAnsport Codes) [12], has been fully tested and is extensively used for the study of ELM dynamics, such as the mechanism of transition from conductive to convective energy loss during ELM [10]. Also, an integrated code TOPICS-IB [11] was coupled with a dynamic five-point model [13] for SOL / divertor plasmas and a stability code for peeling-ballooning modes, MARG2D [14]. The TOPICS-IB is based on a 1.5D core transport code TOPICS extended to the integrated simulation for burning plasmas. The TOPICS-IB was recently used to study the potential mechanism of the ELM energy loss, such as the collisionality dependence of the energy loss caused by the edge bootstrap current and the SOL parallel transport [11].

In this paper, the two integrated core / SOL / divertor transport codes TOPICS-IB and JINTRAC with links to MHD stability codes have been coupled with models of pellet injection to clarify effects of pellet on the ELM behavior. By using both integrated codes, we study two mechanisms of ELM triggering by the pellet, i.e., pellet energy absorption and transport enhancement effects. TOPICS-IB and JINTRAC complement each other in many respects. Simultaneous use of both codes to simulate the same mechanism provides the extra benefit of code benchmarking and ensures consistency of obtained results. In the next section, we explain TOPICS-IB and JINTRAC. In Section 3, pellet penetration depths in simulation results are compared with those estimated in JT-60U and JET experiments, and then the effects of pellet energy absorption and transport enhancement are investigated. We examine if they can reproduce the main experimental observations such as the onset timing of a pellet triggered ELM, the energy loss, the independence of pellet injection location and so on. A summary and discussion are presented in the last section.

2. INTEGRATED MODELING OF PELLET TRIGGERED ELM WITH TOPICS-IB AND JINTRAC

The mechanism of pellet triggered ELM is investigated by the integrated codes TOPICS-IB and JINTRAC. Details of both codes are given in [10-12]. Both codes are coupled with respective pellet models. Both codes treat 1.5D profiles even during the pellet ablation and further drift, and the plasma stability is examined in the profiles including pellet induced perturbations spreading evenly over flux surfaces. Some essential features of codes and models are explained as follows.

2.1 TOPICS-IB

TOPICS-IB is based on the 1.5D core transport code TOPICS, which is coupled with a linear MHD stability code MARG2D, a SOL / divertor five-point model and a pellet model APLEX (Ablated PeLlet with E×B drift). TOPICS solves the 1D transport and current diffusion equations on the normalized toroidal flux coordinate, ρ, and the Grad-Shafranov equation of MHD equilibrium on the 2D plane (R, Z). Particle and thermal diffusivities consist of neoclassical and anomalous contributions, where the anomalous diffusivities are given as empirical formulas. In order to produce

the H-mode pedestal, the transport near the edge is reduced to the neoclassical value calculated by the matrix inversion method [15] with a prescribed pedestal width, Δ_{ped}. The ELM model is developed by coupling TOPICS with MARG2D. In the present simulation, the linear stability of n = 1-50 modes are examined at given time-intervals, where n is the toroidal mode number. When unstable modes appear, an ELM is assumed to occur. The ELM enhanced diffusivities are added on the basis of eigenfunction profiles of unstable modes, where the maximum value, χ_{ELM}^{max}, is given as a parameter. The ELM enhanced transport is maintained for a time interval τ_{ELM} given as a parameter. The five-point model is based on time-dependent Braginskii's fluid equations. Particle flux and heat fluxes across the separatrix obtained in TOPICS are used as inputs and the five-point model calculates the SOL density and temperatures at the separatrix which are used as boundary conditions in TOPICS. The parameters are chosen as $\Delta_{ped} = 0.05$ on the ρ coordinate, $\chi_{ELM}^{max} = 100 m^2/s$ and $\tau_{ELM} = 200 \mu s$ in this paper.

APLEX model is based on equations of pellet ablation, ExB drift of the detached plasma cloud (or plasmoid) and cloud energy absorption. The reduction rate of the pellet radius r_p by the ablation is given as [16],

$$\frac{dr_p}{dt} = -C_p \frac{n_{e\infty}^{1/3} T_{e\infty}^{11/6}}{4\pi n_{solid} Z^{2/3} W^{1/3} r_p^{2/3} \left(\ln \Lambda_{en}\right)^{2/3}} \tag{1}$$

where $C_p = 3.8\times10^{16}\ m^{1/3} eV^{-6/11} s^{-1}$, $\Lambda_{en} = 2T_{e\infty}/7.5$, and $n_{e\infty}$, $T_{e\infty}$, n_{solid}, Z, W denote the background plasma electron density, temperature, the atomic density of the condensed phase, the atomic number and the atomic weight in amu, respectively. The pellet ablation produces a plasma cloud attached to the pellet. Then, the cloud is assumed to be detached by an ExB rotationally driven magnetic interchange instability with the time scale of $\tau_{E\times B} = eB_t r_\perp^2/(0.025T_{e\infty})$ [8], where B_t and $r_\perp$ are the toroidal magnetic field and the cloud radius calculated by using the equation (12) in [8]. After the detachment, the pellet ablation produces again a new attached cloud. These periodic "cloud disruptions" breed a sequence of more than 10 detached clouds. The time derivative of the speed $\upsilon_\perp$ of each detached cloud in the direction of major radius R is given as [8,17,18],

$$\Sigma \frac{d\upsilon_\perp}{dt} = \frac{2}{R}\left(p_c - p_\infty\right) Z_c \alpha(Z_c, q) - \max\left(\frac{2B_t^2 \upsilon_\perp}{\mu_0 c_{A\infty}}, H(t-\tau_\sigma)\frac{\sigma B_t^2 \left(1-e^{-t/t_c}\right) L_b L_l \upsilon_\perp}{2\left(L_t - Z_c\right)}\right) \tag{2}$$

where $\Sigma = m_i n_c Z_c$, $\alpha(Z_c, q) = \cos(Z_c/(R_0 q))\ (\mathrm{sgn}(\pi R_0 q/2 - Z_c)+1)$, $c_{A\infty} = B_t/(\mu_0 m_i n_{i\infty})^{1/2}$, $\tau_\sigma = [\mu_0 \sigma \pi r_\perp^2 \{L_s/(2c_{A\infty})\}^2]^{1/3}$, $L_b = 2r_\perp$, $L_{l//} = 2\min[L_b/4, \{\int_0^t 4\pi/(\mu 0\sigma) dt'^{1/2}]$ and $L_\phi = 4\pi^{3/2} R a/r_\perp$. The first term in the right-hand-side of equation (2) is a driving term due to a vertical curvature and ∇B drift current induced inside the cloud by the 1/R toroidal field variation, which results in the E×B drift [8,17]. The second and third terms are damping terms due to the Alfven wave [8,18] and the external current [18], respectively. In equation (2), the cloud pressure $p_c = 2n_c T_c$ and the half length of the cloud along the magnetic field line $Z_c = L_c + c_s t$ where $L_c = (r_\perp R)^{1/2}$, $c_s = (2\gamma T_c/m_i)^{1/2}$, $\gamma = 5/3$ and m_i is the ion mass. The cloud temperature, T_c, is evaluated from $T_c = E_c/(3N_c)$ where E_c is the

cloud energy and N_c is the total number of cloud particles. The cloud density, n_c, is reduced due to the parallel expansion of the cloud and the perpendicular diffusion, and is obtained by solving $d(n_cZ_c)/dt = -2D_cn_cZ_c/L_n^2$, where the initial density is set by using the equation (8) in [8], the cloud particle diffusivity D_c consists of a classical collision part and an anomalous part D_{can}, and the perpendicular characteristic length L_n is assumed to be equal to r_p. It is beyond the scope of this paper to analyze D_{can} and thus the value of D_{can} is chosen as $D_{can} = 0.04m^2/s$ in this paper so that the APLEX model reproduces pellet penetration depths in JT-60U experiments as will be shown in Section 3. The above D_{can} value is between the classical collisional diffusivity and Bohm one (~0.01 and ~ $0.1m^2/s$, respectively) for typical parameters of cloud plasma with T_c~10eV and n_c~10^{21} m^{-3}. Other variables in equation (2), p_∞, R_0, q, σ, L_s, τ_e and *a* denote the background plasma pressure, the major radius at the magnetic axis, the safety factor, the plasma conductivity, the magnetic shear length, the electron collision time and the minor radius, respectively. When the cloud plasma pressure equilibrates with the background one, $p_c = p_\infty$, the cloud is homogenized with the background plasma. To study the transport enhancement effect during the homogenization, the ad-hoc diffusivity is added to the background plasma transport based on a Gaussian profile within the deposition region. The time derivative of cloud energy E_c is given as [18,19],

$$\frac{dE_c}{dt} = f_s f_d \int q_{e\parallel} dS_\mathrm{P} + \int q_{e\perp} dS_\perp - (p_c - p_\infty) c_s S_\perp \tag{3}$$

where the shielding factor for electrostatic potential $f_s = 0.2$ [8], f_d denotes the deposition factor during passing the cloud [20], the parallel electron heat flux $q_{e//} = n_{e\infty}\{2T_{e\infty}/(\pi m_e)\}^{1/2}(T_{e\infty} - T_c)$ [21], and the perpendicular heat flux is assumed as 1% of $q_{e//}$ [22].

2.2 JINTRAC

JINTRAC includes the pellet ablation and deposition code HPI2, the 1.5D core transport code JETTO and the multi-fluid SOL-divertor code EDGE2D-EIRENE [10,12]. In JETTO, the transport equations are solved for plasma current, temperatures and density. Transport coefficients in the core are calculated according to the mixed Bohm/gyroBohm transport model. The pedestal is established by transport reduction to the neoclassical level within the edge barrier with a prescribed barrier width. If the normalized pressure gradient α exceeds critical value α_{crit} (prescribed by a value obtained from the MHD stability code or an experimentally-evaluated value) anywhere within the pedestal, ELM events are emulated by a temporary sharp increase in edge transport. In the SOL, perpendicular transport is defined by the diffusivities at the separatrix; longitudinal transport follows Braginskii's approximation.

HPI2 determines the pellet particle source by application of a pellet ablation model which is based on the neutral gas and plasmoid shielding description [23]. The E×B drift of the cloudlets can be taken into account following a four-fluids Lagrangian model for the plasmoid homogenisation process [18]. The structure of the drift equation is similar to equation (2):

$$\frac{d\upsilon_{\perp}}{dt}=\frac{1}{1+\left(1-P_{Alf}-P_{con}\right)\left(L'_{con}n_{e\infty}/Z_c n_c\right)}\left\{\frac{2\left(p_c-p_{\infty}\right)}{n_c m_i R}\alpha(Z_c,q)-\frac{\upsilon_{\perp}B^2}{n_c m_i Z_c}\cdot\left[P_{Alf}\frac{2}{\mu_0 c_{A\infty}}+P_{con}\frac{\left[1-e^{-t/\left(\tau_e+\tau_{self}\right)}\right]\pi R_0^2\sigma}{L_{con}}\right]\right\} \quad (4)$$

where P_{Alf}, P_{con}, L_{con}, τ_{self}, and L'_{con} denote the fraction propagating along the field line at the Alfven velocity, the connecting fraction between regions of opposite polarization caused by the vertical toroidal drift, the length of connecting flux tube, the ratio between the self-inductance and the resistance of a circuit produced by the connection, the flux tube length drifting by the E×B drift, respectively. A detailed description of equation (4) is given in [24]. In HPI2, the heat transfer from the background plasma to the plasmoid is governed by the following equations, which describe the change in electron and ion energy content of the plasmoid [18]:

$$\frac{dE_c^{e/i}}{dt}=Q_{\infty c}^{e/i}+Q_c^{ie/ei}+\frac{1}{N_c}\frac{dN_c}{dt}E_c^{e/i}+W_c^{e/i}-p_c^{e/i}S_{\perp}\frac{dZ_c}{dt} \quad (5)$$

The first term in the right-hand-side of equation (5) describes the heat exchange between the plasmoid and the background plasma in the magnetic flux surface shell, where the plasmoid is located. The other terms in equation (5) account for the electron-ion energy equilibration, and losses due to the convection, viscosity and expansion work.

HPI2 is more detailed in comparison with APLEX model in TOPICS-IB in the following respects; (1) treating cloud ion temperature T_{ci} and electron one T_{ce} separately (also taking account of ion heat flux) ($T_{ci}=T_{ce}$ assumed and no ion heat flux in APLEX), (2) taking account of detailed perpendicular heat flux (constant fraction of $q_{e//}$ assumed in APLEX), (3) taking account of expansion of cloud radius (constant cloud radius assumed in APLEX).

3. INTEGRATED SIMULATION RESULTS

TOPICS-IB and JINTRAC complement each other in many respects. Simultaneous use of both codes to simulate the same mechanism provides the extra benefit of code benchmarking and ensures consistency of obtained results. Parameters used in the simulations are as follows; $R = 3.3$m, $a = 0.72$m, $\kappa = 1.7$, $\delta = 0.086$, $I_p = 1.5$MA, $B_t = 3.5$T for the JT-60U ELMy H-mode experiment [25] and $R = 2.9$m, $a = 0.91$m, $\kappa = 1.7$, $\delta = 0.35$, $I_p = 1.7$MA, $B_t = 2.0$T for the JET ELMy H-mode experiment [26].

3.1. COMPARISON OF PELLET PENETRATION DEPTH AMONG CODES AND EXPERIMENTS

We first compare pellet penetration depths among simulation and experimental results in order to verify and validate the codes. Figure 1 shows electron density n_e profiles just before and 3 ms after the injection of a deuterium pellet from the high-field-side top (HFStop) with the initial pellet size $r_{p0} = 0.6$mm and the speed $\upsilon_p = 120$m/s in TOPICS-IB and JINTRAC simulations for the JT-60U H-mode experiment. In figure 1, the region in which the density increases qualitatively agrees with

that in the experiment. The deposition depth in the TOPICS-IB simulation, which uses ExB drift, is about 0.2 in terms of the ρ coordinate, which is close to the depth experimentally estimated by the electron-cyclotron-emission measurement. The deposition depth in the JINTRAC simulation is slightly deeper (~0.3). When the E×B drift and the time-dependent interaction between the pellet and the background plasma are switched off, which is the same condition as the conventional ablation calculation, the deposition (or ablation) depth is about 0.05 in both TOPICS-IB and JINTRAC. Thus, the radial displacement by the E×B drift is about 0.15 for TOPICS-IB and about 0.25 for JINTRAC in this case of HFS pellet injection.

The comparison of deposition depth between TOPICS-IB and JINTRAC is also done for a pellet from the Vertical HFS (VHFS) and the Low-Field-Side (LFS) with $r_{p0} = 0.55$mm and $\upsilon_p = 130$m/s in JET L-mode experiment [12] ($R = 2.9$m, $a = 0.89$m, $\kappa = 1.6$, $\delta = 0.21$, $I_p = 2.0$MA, $B_t = 2.3$T) as shown in figure 2. The deposition behavior appearing in the change of electron density profile for the various size of pellet could be roughly reproduced by JINTRAC simulations [12]. In the VHFS case of figure 2(a), the deposition depth in the JINTRAC simulation is about 0.29, which is close to the estimated depth in the experiment. The depth in the TOPICS-IB simulation is slightly shallower (~0.25). When the E×B drift and the time-dependent interaction are switched off, the deposition (ablation) depth is almost the same between JINTRAC and TOPICS-IB (~0.23 and ~0.22, respectively). The radial displacement by the E×B drift is about 0.06 for JINTRAC and about 0.03 for TOPICS-IB in this case. Both values of radial displacement are small due to the low beta in the L-mode plasma compared with those in the above H-mode. On the other hand, in the LFS case, the ExB drift shifts the deposition outward and the deposition depth is determined mainly by the pellet ablation. In figure 2(b), the deposition depth in both codes is about 0.3, which is close to the experimentally estimated depth, regardless of the model assumption such as the ExB drift on or off. From these comparisons, the prediction of ablation depth is almost the same between TOPICS-IB and JINTRAC, but the prediction of radial displacement by the ExB drift seems a little different, i.e., the depth predicted by TOPICS-IB is shallower than JINTRAC. The further comparison with experiments is necessary for the improvement of prediction accuracy of codes. Although the above difference exists between TOPICS-IB and JINTRAC, both codes show that the same mechanism triggers the ELM as described below.

3.2 ELM TRIGGERED BY PELLET ENERGY ABSORPTION

The effect of pellet energy absorption on the ELM is examined. Figure 3 shows the time evolution of background total pressure profile in the TOPICS-IB case of figure 1, but with the ELM model switched off. The pellet cloudlet absorbs the background plasma energy at the magnetic flux surface, which the cloudlet crosses. The ExB drift shifts inward the heated cloudlet and deposits its energy in a region, where the cloud merges with the background plasma. The energy absorption and the following ExB drift modify the background plasma profile and produce a region with steeper pressure gradient in figure.3. The drop of electron temperature besides the adiabatic drop is about 10 % of

temperature before the pellet injection, which almost agrees with the experimental observation [6].

Figures 4(a-c) show the same case with the ELM event enabled, where results in "natural" ELMs (without the pellet injection) are also shown in figures 4(d-f). In figures 4(b) and (e), the normalized pressure gradient α is defined as $\alpha = -2\mu_0(a\rho)^2/B_p\ (dP/d\psi)$ where B_p and ψ denote the poloidal magnetic field and the poloidal flux function, respectively. The local steep pressure gradient occuring within the pedestal can destabilize the high-n ballooning mode ($n > 40$ in this case) and trigger an ELM in figures 4(a-c). Indeed, the local value of α in figure 4(b) exceeds that in "natural" ELMs ($13 \leq n \leq 28$ unstable) in figure 4(e). The width of eigenfunction profile is narrower in the pellet triggered ELM than that in "natural" ELMs (comparing figure 4(c) with (f)). The region of ELM enhanced transport almost corresponds to the pedestal region independently of position at which the pellet triggers the ELM. The resultant energy loss is less than half of the "natural" ELMs as shown in figure 5. This reduction of ELM energy loss agrees with experimental observations in ASDEX Upgrade [4,5] and DIII-D [27]. We have also performed simulations with a LFS pellet and obtain similar results.

Figure 6 shows the time evolution of profiles of (a) P, (b) α and (c) heat source and sink by the energy absorption effect of a VHFS pellet with $r_{p0} = 0.9$mm and $\upsilon_p = 150$m/s in a JINTRAC simulation for the JET experiment. The pressure redistribution by the pellet energy absorption and the subsequent E×B drift leads to an increase of pressure gradient, triggering an ELM at $7.3402\text{s} < t < 7.3404\text{s}$. At this time, the pellet has not yet reached the pedestal top. Figure 7 shows the time evolution of (a) volume-averaged electron density n_{eav} and (b) stored energy W_s for repetitive VHFS pellets with 50 Hz from $t = 7.34$s. ELMs are triggered every time when pellet is injected.

3.3 ELM TRIGGERED BY PELLET TRANSPORT ENHANCEMENT

We next investigate the effect of pellet transport enhancement. Figure 8 shows profiles of plasma pressure, normalized pressure gradient and ion heat diffusivity just before and 100μs after the HFS pellet injection in a JINTRAC simulation without the energy absorption effect for the JET experiment. In the simulation, to study the pellet transport enhancement effect, the instantaneous pellet deposition is assumed and the transport is enhanced in the vicinity of deposition region for 100μs following the deposition. In the model of the pellet transport enhancement, the magnitude is much less than the ELM enhanced transport but larger than the stationary value, and the duration is based on the experimental observation in which ELMs were triggered about 50μs after the pellet imposed the seed perturbation [5,7]. If the region with the enhanced transport spreads over the pedestal top, it can also lead to a sudden reduction of pedestal width. The transient transport enhancement and the resultant pedestal contraction are shown to be able to create a narrow region with the steep pressure gradient close to the pedestal top in figure 8. This results in the prompt onset of ballooning instability and ELM by using the same criteria in previous subsection. Figure 9 shows a JINTRAC simulation result of the time evolution of stored energy, volume-averaged density and D_α emission for a string of pellets starting from $t = 7.4$s. Note that infrequent strong ELM crashes

before t < 7.4s are due to “natural” ELMs. Each pellet triggers an ELM crash if the pellet injection frequency does not exceed 200Hz. ELM triggering becomes unreliable (not each pellet triggers the ELM) if pellet repetition rate exceeds 200Hz. Also, pellet does not reliably trigger ELM (in both experiment and modelling) if the distance between previous “natural” ELM and further pellet ablation is shorter than $\Delta t < \sim 3$ms.

Figure 10 shows the time evolution of (a) P and (b) χ_e profiles with the pellet transport enhancement effect used in TOPICS-IB code for the same case as figure 1, but with the pellet energy absorption effect and the ELM model switched off. In this simulation, it was assumed that a series of cloudlets enhances transport for 10μs following the deposition as shown in figure 10(b) and creates the pressure perturbation in figure 10(a). Figure 11 shows the same case with the ELM event enabled. Almost as in the case of figure 4, high-n modes become unstable and the eigenfunction profiles are narrow compared with those in the "natural" ELM. The ELM energy loss triggered by the pellet is less than half of that in the "natural" ELM. Similar results are also obtained in simulations with a LFS pellet. When both the pellet energy absorption and the transport enhancement are taken into account in the TOPICS-IB simulation, the pellet makes the background pressure perturbation even stronger and triggers ELM more reliably. Either effect triggers high-n modes, with the narrowness of eigenfunction profiles and the magnitude of ELM energy loss being almost the same in both cases.

SUMMARY AND DISCUSSIONS

Two integrated core / SOL / divertor transport codes TOPICS-IB and JINTRAC with links to MHD stability codes have been coupled with pellet models to clarify effects of pellet on the ELM behavior. Both codes predicted the following two triggering mechanisms. Both the energy absorption and the transport enhancement by the pellet were found to be able to trigger the ELM. The ablated cloud of pellet absorbs the background plasma energy and causes a radial redistribution of pressure due to the subsequent ExB drift. On the other hand, the sharp increase in local density and temperature gradients in the vicinity of ablated cloud causes the transient enhancement of heat and particle transport. Both mechanisms produce a region of increased pressure gradient in the background plasma profile within the pedestal, which triggers the ELM. Simulations show that the two considered mechanisms have the potential to explain a wide range of experimentally observed phenomena.

The simulation and the model validation on other sets of parameters (not only different plasmas but also different machines such as ASDEX Upgrade) remains as future work. The two mechanisms discussed above may fail to trigger the ELM for lower pedestals with lower pressure gradients, which appears just after the ELM collapse. Additionally, in the present simulation, one pellet triggered one instability only. It is not clear that one pellet can trigger continuous instabilities. Sensitivity studies including the above cases will be done and compared more with experiments (trigger timing, energy loss, mode number, pellet penetration depth, etc.) and also with nonlinear simulations such as in [28]. In the present model, the plasma stability is examined in 1.5D profiles including pellet induced

perturbations spreading evenly over flux surfaces. Thus, simulation results should be compared with those in the nonlinear simulations which can take account of local strong perturbations before the perturbations have the time to spread out. The model improvement, such as the dependence of pellet transport enhancement on the pellet size (or produced density/temperature gradient) and location (HFS or LFS, because instability/turbulence is generally strong in LFS), is necessary. In experiments and nonlinear simulations [28,29], the filamentary structure is formed in the pedestal region and propagates radially from the pedestal into the SOL. The five-point model in TOPICS-IB and the EDGE-2D code in JINTRAC for SOL-divertor plasmas can deal with the parallel transport in the filamentary structure. However, these model/code may not reproduce the radial propagation of filamentary structure from the pedestal into SOL, because of simplified radial transport in the model/code. Although the present model/code reproduced several experimental observations such as the collisionality dependence of ELM energy loss [11], the modeling of filamentary structure needs to be considered for further improvement of model accuracy. By using integrated codes, we will develop the operation scenario considering the consistency between fueling and ELM pacing pellets both to improve the core plasma performance and to reduce the ELM energy loss.

ACKNOWLEDGEMENTS

We are grateful to JT-60 and JET team members for collaboration. This work was partly supported by JSPS, Grant-in-Aid for Scientific Research. This work was also carried out under the collaborating research program at National Institute for Fusion Science. One of authors (N.H.) would like to thank Drs R. Ishizaki, Y. Tomita and A. Takayama for fruitful discussion and taking care of the NIFS program. N.H. is also grateful to Dr. M. Honda and Mr. I. Kamata for developing TOPICS-IB. This work was partly supported by EURATOM and carried out within the framework of the European Fusion Development Agreement. The views and opinions expressed herein do not necessarily reflect those of the European Commission.

REFERENCES

[1]. Baylor L.R. et al. 2007 Nuclear Fusion **47** 1598
[2]. Kim Ki Min et al. 2010 Nuclear Fusion **50** 055002
[3]. Lang P.T. et al. 2008 Nuclear Fusion **48** 095007
[4]. Urano H. et al. 2005 Journal Plasma Fusion Results **81** 280
[5]. Kocsis G. et al. 2007 Nuclear Fusion **47** 1166
[6]. Kocsis G. et al. 2008 35th EPS Conf. on Plasma Physics (Hersonissos, Crete, Greece 2008) vol 32D (ECA) P-2.070
[7]. Szepesi T. et al. 2009 Plasma Physics and Controlled Fusion **51** 125002
[8]. Parks P.B., Sessions W.D. and Baylor L.R. 2000 Physics of Plasmas **7** 1968
[9]. Valovic M. et al. 2008 Nuclear Fusion **48** 075006
[10]. Wiesen S. et al. 2008 Contributions to Plasma Physics **48** 201
[11]. Hayashi N. et al. 2009 Nuclear Fusion **49** 095015

[12]. Koechl F. et al. 2010 37th EPS Conf. on Plasma Physics (Dublin, Ireland 2010) vol 34 (ECA) O4.123
[13]. Hayashi N et al. 2007 Journal Nuclear Materials **363-365** 1044
[14]. Aiba N et al. 2007 Nuclear Fusion **47** 297
[15]. Kikuchi M, Azumi M, Tsuji S, Tani K and Kubo H 1990 Nuclear Fusion **30** 343
[16]. Parks P.B. and Rosenbluth M.N. 1998 Physics of Plasmas **5** 1380
[17]. Senichenkov I.Yu. et al. 2006 Nuclear Fusion **46** 788
[18]. Pegourie B. et al. 2007 Nuclear Fusion **47** 44
[19]. Gal K. et al. 2008 Plasma Physics and Controlled Fusion **50** 055006
[20]. Ishizaki R. et al. 2004 Physics of Plasmas **11** 4064
[21]. Pegourie B. et al. 1996 Physics of Plasmas **3** 4594
[22]. Milora S.L. et al. 1995 Nuclear Fusion **35** 657
[23]. Pegourie B. et al. 2005 Plasma Physics and Controlled Fusion **47** 17
[24]. Commaux N. et al. 2010 Nuclear Fusion **50** 025011
[25]. Takenaga H. and JT-60 Team 2001 Physics of Plasmas **8** 2217
[26]. Lang P. et al. "ELM pacing investigations at JET with the new pellet launcher" in Fusion Energy 2010 (Proc. 23rd Int. Conf. Daejeon, 2010) (Vienna: IAEA) CD-ROM file EXS/P3-03 and http://www-naweb.iaea.org/napc/physics/FEC/FEC2010/html/index.htm
[27]. Baylor L.R et al. 2010 37th EPS Conf. on Plasma Physics (Dublin, Ireland 2010) vol 34A (ECA) P-2.117
[28]. Huysmans G.T.A. et al. "Non-linear MHD Simulations of Natural and Pellet Triggered ELMs" in Fusion Energy 2010 (Proc. 23rd Int. Conf. Daejeon, 2010) (Vienna: IAEA) CD-ROM file THS/7-1 and http://www-naweb.iaea.org/napc/physics/FEC/FEC2010/html/index.htm
[29]. Snyder P.B, Wilson H.R and Xu X Q 2005 Physics of Plasmas **12** 056115

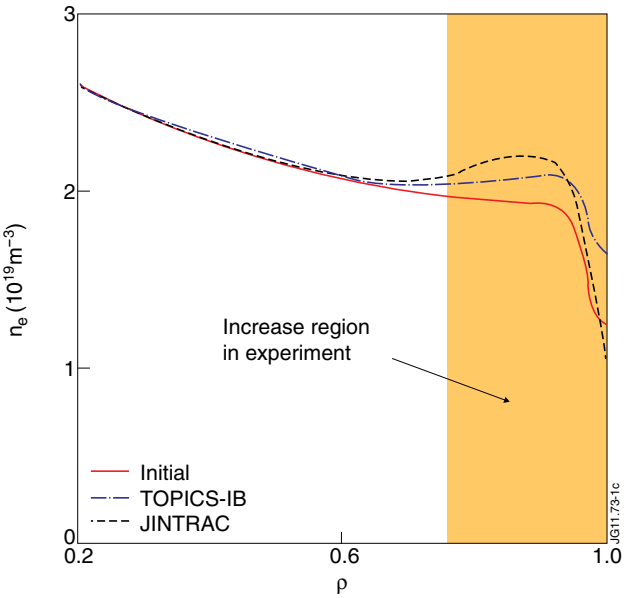

Figure 1. n_e profile before (red solid curve) and 3ms after a HFStop pellet injection in TOPICS-IB and JINTRAC simulations (blue broken and black dotted curves, respectively) for JT-60U experiment where shaded area denotes density increase region observed in experiment.

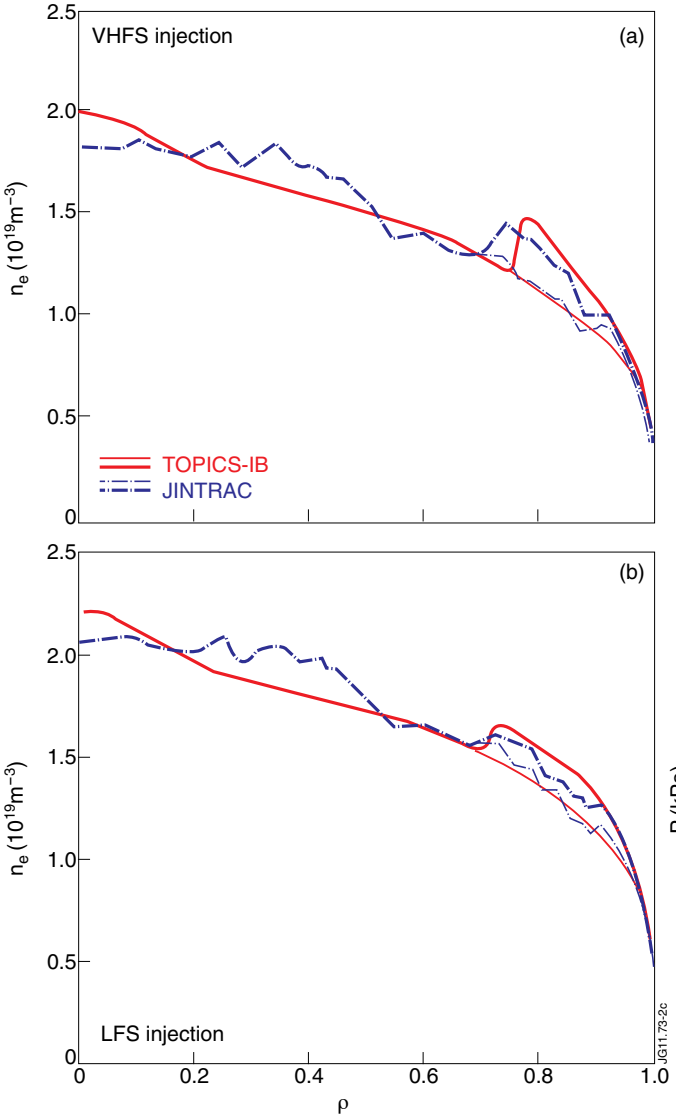

Figure 2. n_e profile before (thin curves) a pellet injection from (a) VHFS and (b) LFS and after pellet deposition (thick curves) in TOPICS-IB and JINTRAC simulations (red solid and blue broken curves, respectively) for JET L-mode experiment. Measured profiles are used as initial ones in JINTRAC, while approximate profiles in TOPICS-IB.

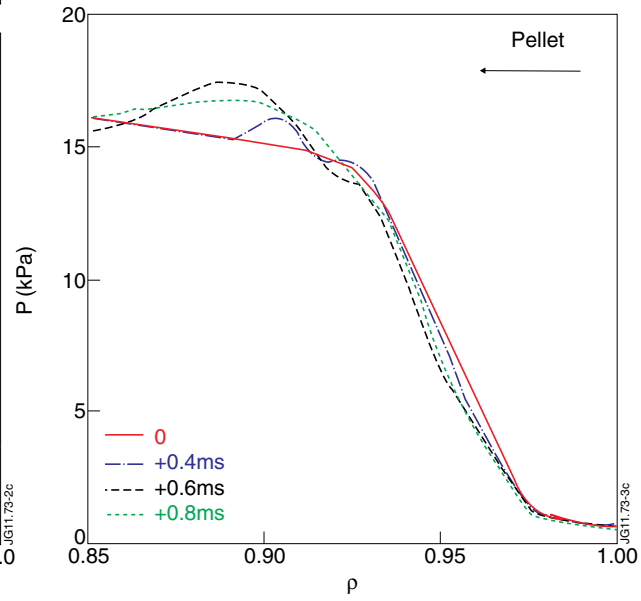

Figure 3. Time evolution of background total pressure P profile in case of figure 1 with ELM model switched off.

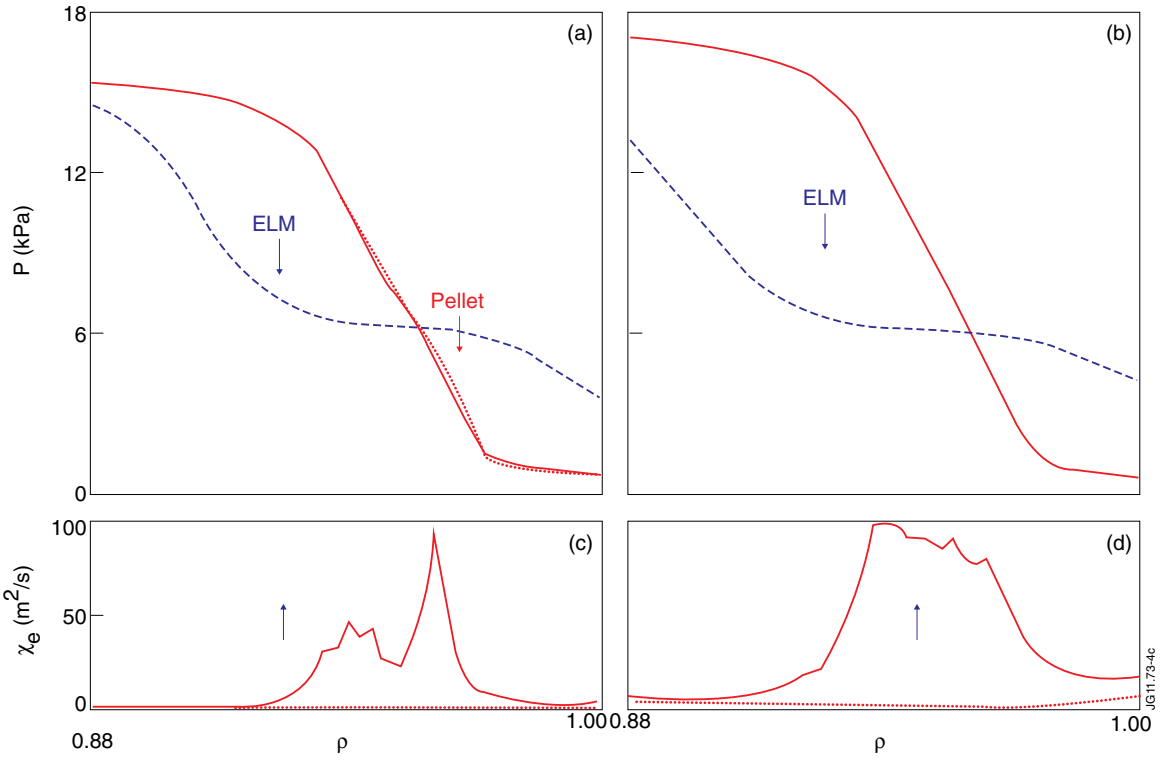

Figure 4. Profiles of (a) P, (b) normalized pressure gradient α and (c) electron heat diffusivity χ_e just before pellet injection (dotted line), at onset of pellet triggered ELM (solid line) and after an ELM (dashed line) in which diffusivity is enhanced during 200μs for case of figure 1 with ELM model. (d)(e)(f) P, α and χ_e profiles in a case of "natural" ELM at ELM onset (solid line) and after an ELM (dashed line).

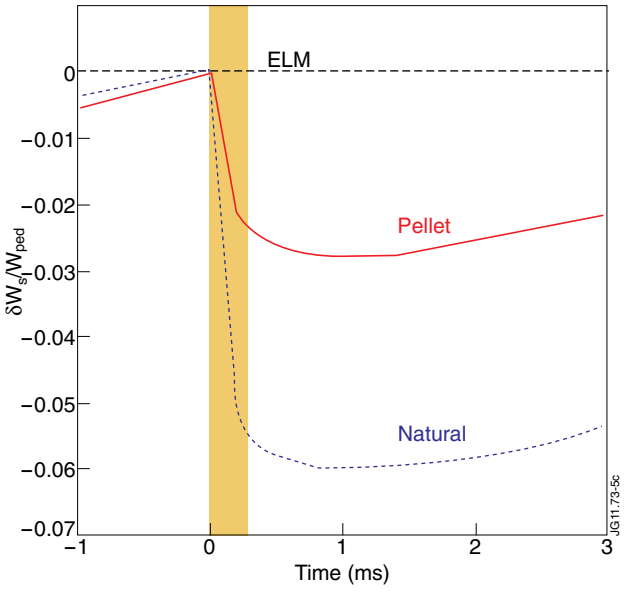

Figure 5: Time evolution of energy loss δW_s normalized by pedestal energy W_{ped} for two cases in figure 4, pellet triggered ELM and "natural" ELM.

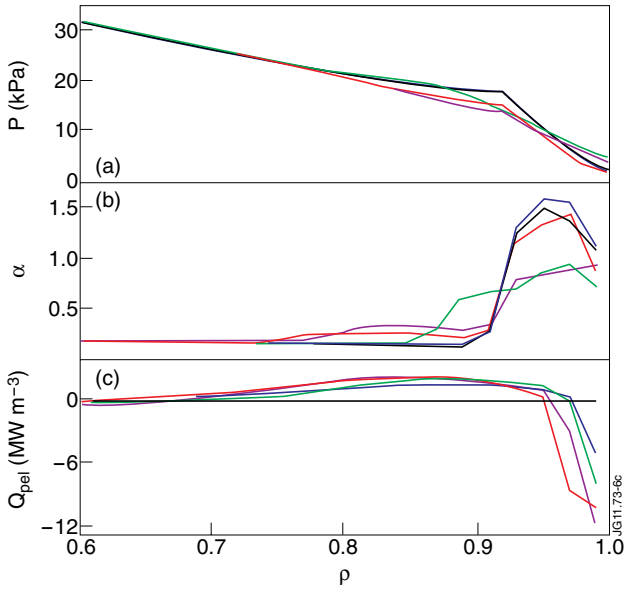

Figure 6: Time evolution of profiles of (a) P, (b) α and (c) heat source and sink Q_{pel} by VHFS pellet in a JINTRAC simulation for JET experiment without pellet transport enhancement (black: 7.3399s, blue: 7.3402s, green: 7.3405s, magenta: 7.3408s, red: 7.3411s).

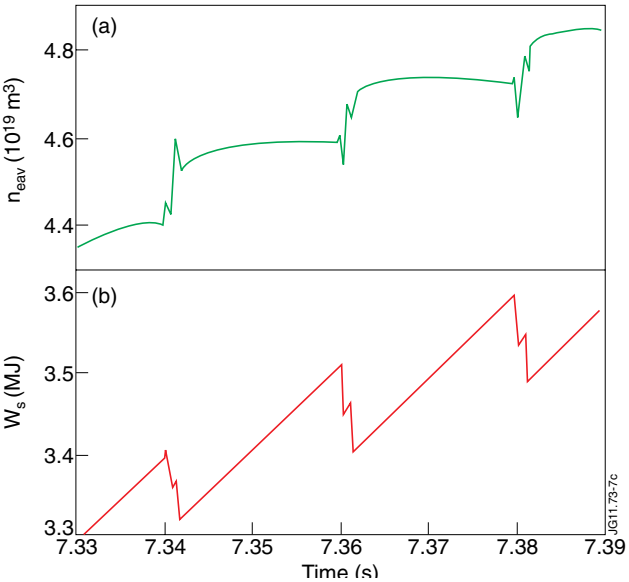

Figure 7: Time evolution of (a) n_{eav} and (bb) W_s for repetitive VHFS pellets with 50Hz from t=7.34 s in a JINTRAC simulation. Time evolution of profiles during first pellet is shown in figure 6.

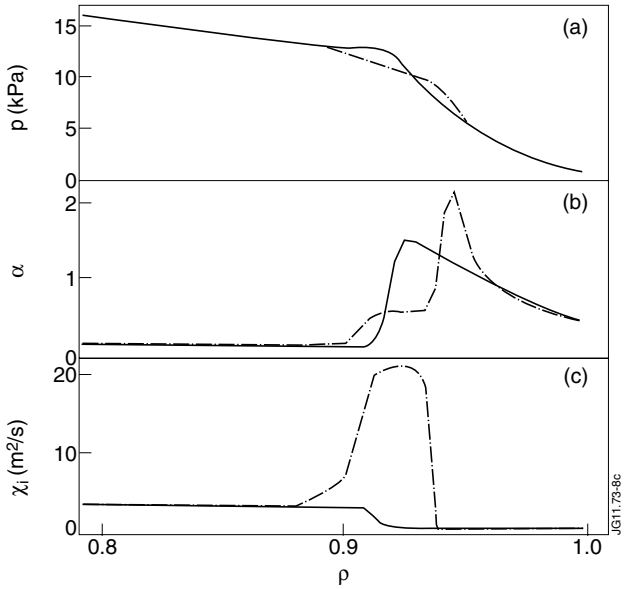

Figure 8: Profiles of (a) P, (b) a and (c) ion heat diffusivity χ_i just before (solid line) and 100ms after (chain line) VHFS pellet injection in a JINTRAC simulation for JET experiment where transport is enhanced in vicinity of pellet deposition.

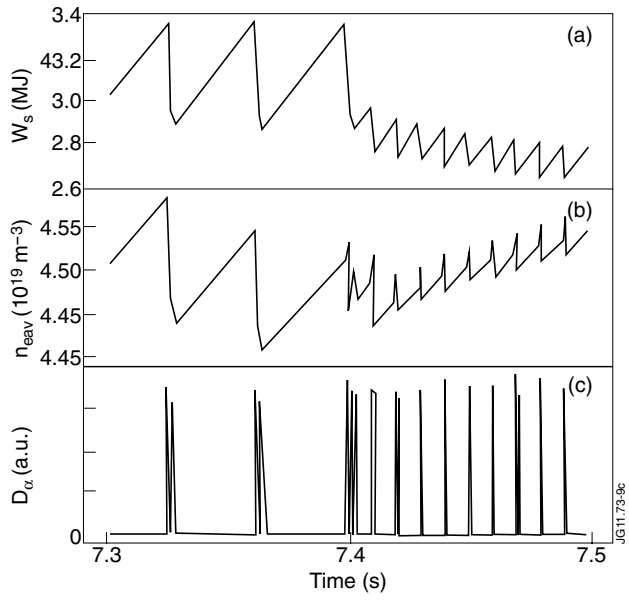

Figure 9. Time evolution of (a) W_s, (b) neav and (c) D_α emission for repetitive pellet with 100 Hz from t = 7.4s in a JINTRAC simulation. ELMs before t = 7.4s are "natural" ELMs. Time evolution of profiles during first pellet is shown in figure 8.

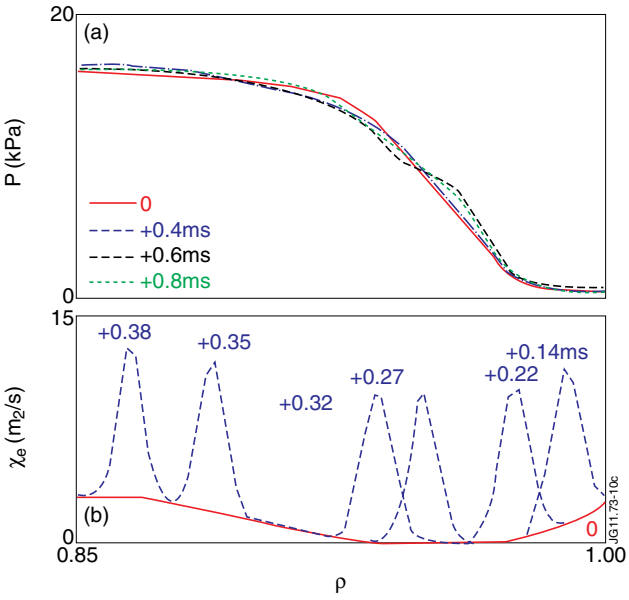

Figure 10. Time evolution of (a) P and (b) χ_e profiles with pellet transport enhancement effect in the same case as figure 1 where pellet energy absorption effect and ELM model are switched off.

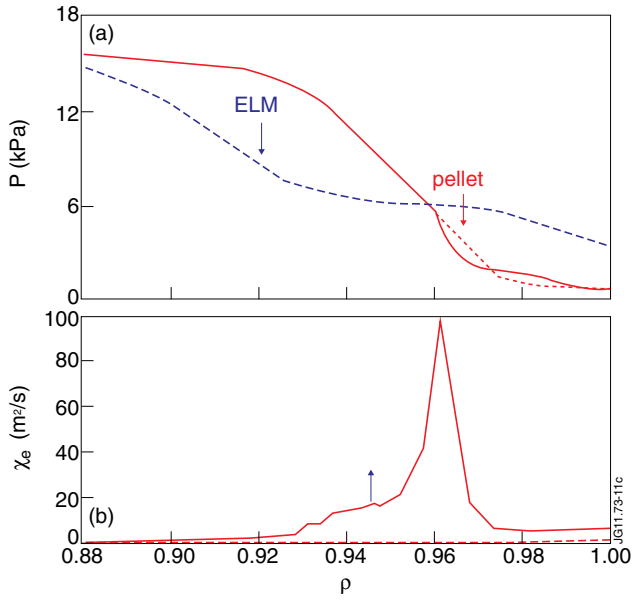

Figure 11. Time evolution of profiles of (a) P and (b) χ_e just before pellet injection (dotted line), at onset of pellet triggered ELM (solid line) and after an ELM (dashed line).